UC-404
LBL-25022
c.1

Center for Advanced Materials

CAM

Presented at the Conference of the American Welding Society,
New Orleans, LA, April 17–22, 1988

RECEIVED
LAWRENCE
BERKELEY LABORATORY

JUL 26 1988

LIBRARY AND
DOCUMENTS SECTION

Weldability of 2090 Al-Cu-Li Alloy

A.J. Sunwoo and J.W. Morris, Jr.

April 1988

For Reference

Not to be taken from this room

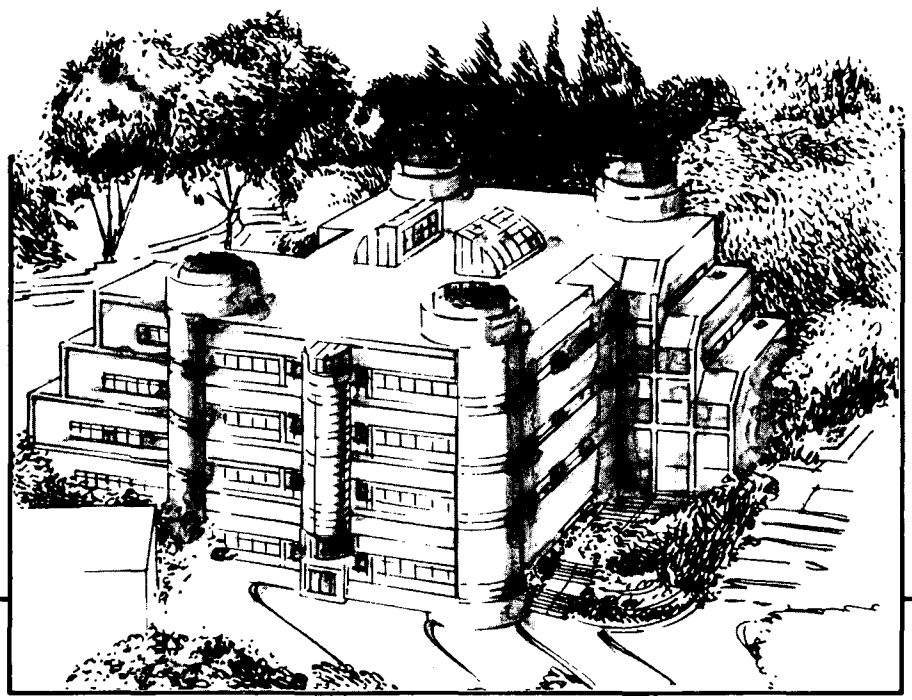

Materials and Chemical Sciences Division

Lawrence Berkeley Laboratory • University of California

ONE CYCLOTRON ROAD, BERKELEY, CA 94720 • (415) 486-4755

Prepared for the U.S. Department of Energy under Contract DE-AC03-76SF00098

LBL-25022 c.1

DISCLAIMER

This document was prepared as an account of work sponsored by the United States Government. While this document is believed to contain correct information, neither the United States Government nor any agency thereof, nor the Regents of the University of California, nor any of their employees, makes any warranty, express or implied, or assumes any legal responsibility for the accuracy, completeness, or usefulness of any information, apparatus, product, or process disclosed, or represents that its use would not infringe privately owned rights. Reference herein to any specific commercial product, process, or service by its trade name, trademark, manufacturer, or otherwise, does not necessarily constitute or imply its endorsement, recommendation, or favoring by the United States Government or any agency thereof, or the Regents of the University of California. The views and opinions of authors expressed herein do not necessarily state or reflect those of the United States Government or any agency thereof or the Regents of the University of California.

LBL # 25022

Weldability of 2090 Al-Cu-Li Alloy

A. J. Sunwoo and J. W. Morris, Jr.

Center for Advanced Materials
Materials and Chemical Science Division
Lawrence Berkeley Laboratory
University of California
Berkeley, California 94720

April 1988

This work is jointly supported by the Director, Office of Energy Research, Office of Basic Energy Science, Materials Sciences Division of the U. S. Department of Energy under Control No. DE-AC03-76SF00098

Weldability of 2090 Al-Cu-Li Alloy

A. J. Sunwoo and J. W. Morris, Jr.

Center for Advanced Materials, Lawrence Berkeley Laboratory, and
Department of Materials Science and Engineering, University of California, Berkeley

The weldability of 2090 was studied along with the metallurgical changes associated with welding and aging. Autogenous bead-on-plate welds are produced using two different base metal tempers, as-received condition (T3) and peak-aged condition (T8), and two different welding processes, GTAW and EBW. The optimum aging condition is determined for the EB and GTA weldments. The results of weldability and aging studies indicate that the best aging temperature for the base metal and EB weldments is 160°C, which results in a 75% joint efficiency and for the GTA weldment is 190°C, which produces a 55% joint efficiency. Aging at 230°C leads to a serious deterioration in the properties. The distribution of precipitates in the fusion zone appears to be the primary factor in controlling the weldment strength and elongation.

Introduction

The alloy 2090-T8E41 has superior mechanical properties to current commercially available high strength aluminum alloys at room and cryogenic temperatures [1,2], and has properties competitive with those of 7075 at room temperature. The combination of high specific strength and toughness and high specific modulus are of interest to the aircraft and aerospace industries. Some of the more promising applications of 2090 are in weight-critical cryogenic structures, such as fuel tanks for advanced aircraft, and the external liquid fuel tanks of the space shuttle. Since these applications require welding, the weldability of 2090 needs to be investigated.

The welds produced on an earlier generation of Al-Li alloys were highly susceptible to porosity and hot cracking [3,4]. However, with improved fabrication and processing techniques, many of these problems have been eliminated [5]. In 2090, the source of the gas that causes porosity is probably hydrogen evolving from hydrated oxide on the surfaces of the plate, or from lithium hydride stringers within the material [6]. Gas is trapped during welding. Hence, porosity can be minimized by surface cleaning and by degassing the plate prior to welding [7,8].

Hot cracking, on the other hand, was initially theorized to be a rupture caused by a large solidification range and a critical shrinkage strain [9]. Hence the hot cracking susceptibility is expected to be the highest at the composition of maximum solid-solution solubility. However, Cross, et al. [10] showed that a binary Al-Li alloy with maximum solid-solution solubility of 4.0 wt-% Li is most susceptible to hot cracking at 2.6 wt-% lithium. Similarly, the hot cracking susceptibility of an Al-Cu alloy with maximum solubility of 6 wt-% Cu is greatest at about 3 wt-% Cu [11]. According to Pumphrey, et al. [9,11], when the Cu content is low, less than 1 wt-%, continuous eutectic films will not form at the dendrite boundaries. When the Cu content is very high, cracking will not occur since there is sufficient eutectic liquid to back fill and heal the cracks. However, at 3 wt-% Cu, just enough liquid remains to form continuous films between the grains. Borland, and Clyne and Davies [12, 13] modified the the previous concepts and suggested that hot cracking is influenced by the wettability of dendrites by interdendritic eutectic liquid as well as the

time available to back fill and heal the crack. The Cu and Li contents of 2090 are similar to those in the binary alloys that are highly susceptible to hot cracking. Hot cracking was observed during GTA welding, and in addition, porosity was present in the fusion zone. The methods used to prevent these problems are discussed briefly.

The purpose of this work was to study the weldability of 2090 alloy and the metallurgical changes associated with welding and aging. Since the effects of aging on weldments has not been investigated, aging behavior will be examined to determine the optimum heat treatment for the 2090 weldments.

Experimental Procedure

The chemical composition of as-received 2090 in wt-% is 3.0Cu-2.2Li-0.2Zr-Al. The as-received 2090 sheet was in the solution heat treated and stretched temper, T3. The sheet was cut into the weld coupons of 102 mm x 203 mm (4 in. x 8 in.). The weld coupons were machined down from their initial thickness of 4.3 mm (0.17 in.) to approximately 3.2 mm (0.12 in.) in order to remove distortion and processing oxide. Prior to welding, the weld coupons were chemically cleaned using 5 vol. % NaOH in water, followed by concentrated nitric acid.

Autogenous, bead-on-plate welds were produced transverse to the rolling direction using two different base metal temper conditions, as-received (T3) and peak-aged (T8), and two different welding processes, gas tungsten arc (GTA) and electron beam (EB) welding. These processes were chosen to study the effects of fusion zone microstructures as well as the effects of solute segregation on properties, since there is a significant difference between the cooling rates of these two processes. Welding parameters for GTAW and EBW are listed in Table 1. For GTA welding, direct current straight polarity (DCSP) was utilized, and welding was conducted on a water-cooled chill block in an argon atmosphere.

The base metal and weldments of T3 temper were aged at 160°C, 190°C, and 230°C, to obtain T8 temper. In addition to the post-weld aged conditions, the solution heat treated and aged (SHT&A) conditions of the base metal and both weldments were also investigated. The optimum temperatures for SHT were determined using differential scanning calorimetry. SHT&A consists of a three-step heat treatment: 535°C for 15min, 550°C for 15min, water quench, and subsequent aging at 160°C. Figure 1 shows the tensile specimen configurations.

TEM specimens were prepared by polishing the disks to 0.125 mm thickness and jet-electropolished using 75 vol.% methanol and 25 vol.% nitric acid solution at -30°C. The foils were viewed at 100 kV.

Results

Mechanical Properties

The yield strength, ultimate tensile strength (UTS), and elongation of base metal, EB weldments, and GTA weldments are presented in Table 2. The results of the aging study indicate that 2090 strength degrades after exposure at temperatures greater than 200°C. The best overall

strength and elongation combination for the base metal follows aging at 160°C. As aging time increases from 16 hours to 32 hours, the yield strength continues to increase while the UTS decreases slightly with no changes in total elongation. The base metal aged at 190°C shows no significant improvement in the properties. However, specimens aged at 230°C are severely overaged; the yield strength decreases to less than 50% of the 160°C peak-aged condition, and the elongation has the lowest value of all aging conditions.

For EB weldments, the highest strengths are obtained by aging at 160°C for approximately 32 hours. The aging behavior of the EB weldments is similar to that of the base metal when aged at 190°C and at 230°C. When the peak yield strength at 160°C is compared to that at 190°C and 230°C, the weldment strength decreases from 410 MPa to 340 MPa and to 290 MPa, respectively. The aging behavior of GTA weldments, on the other hand, indicates higher yield strengths at 190°C than at 160°C. However, the peak yield strength at 190°C is reached between 16 and 24 hours, while the yield strength of weldments aged at 160°C continues to increase and peaks beyond 32 hours. Aging at 230°C also adversely affects GTA weldment properties. The joint efficiencies of EB and GTA weldments in the near peak aged condition are 75% and 55%, respectively.

As presented in Table 2, EB and GTA weldment elongations are significantly lower than those of base metal, especially in the aged condition. Visual observation of the tested as-welded EB and GTA specimens reveal severely localized deformation at the fusion zones and minimal deformation in other areas. Since there is a significant difference in strength between the base metal and weld, the effect of the strength incompatibility on the effective elongation was investigated. For the as-welded EB and GTA weldments with the T3 base metal temper, the elongation is 4.4%; however, with the T8 temper the as-welded weldment elongation decreases to 1.3% and 3.6%, respectively. Thus, a part of the decreased weldment elongation is caused by the strength incompatibility. In order to eliminate the strength incompatibility between the base metal and weld, GTA specimens composed only of weld metal were tested (Figure 1b). In the as-welded condition, the all-weld metal specimens elongated 17% in comparison to 4.4% elongation of the composite specimens. In the peak-aged condition, the all-weld metal specimens exhibit only 1.5% elongation; however, this value is still higher than the composite specimen elongation of 0.8%. The results of all-weld metal specimens indicate that the effective elongation of the weldments is much less than the actual elongation of the fusion zone.

The differences in the strengths of the longitudinal and composite specimens depend on the aging conditions. In the as-welded condition, the strength of the longitudinal weld specimens is 17% higher than that of the composite specimens. In the peak-aged condition, the strength of the composite specimens is 16% higher.

The strength incompatibility may have some effect on the weldment elongation, but other mechanisms must also be associated with controlling weldment elongation since the elongation consistently decreases with aging. In order to homogenize the solute distribution in the weld and to erase prior thermal mechanical processing of the base metal, the weldments as well as the base metal are solution heat treated and aged. The strengths of the base metal and weldments aged for 4 hours at 160°C are almost same, and EB weldment elongation increases to 5.4%. As the aging time increases to 16 hours, EB weldment elongation decreases to 1.8%, while the difference in

strength between the EB weldment and base metal is small. GTA weldment elongation did not improve. The results again show that other microstructural factors are responsible for low weldment elongation in the aged conditions.

Fractography

SEM fractographs show different fracture modes for the base material, EB weldments, and GTA weldments. In general, the base material fractures in shear. Figure 2 shows the SEM fractographs of the base metal in peak-aged and overaged conditions. In the peak-aged condition, the fracture surface appears planar-transgranular whereas in the over-aged condition, the surface appears ductile with subgrain delamination. The fracture mode and failure location in the EB weldments change with aging condition. Figure 3 shows EB fracture surfaces in the as-welded, peak aged, and SHT&A conditions. The fracture surface of as-welded EB specimens indicates ductile fracture with void formation and slip evident, Figure 3a. Failures occur at the fusion boundary. In the peak aged condition, the fracture surface reveals interdendritic fracture, Figure 3b, and failures occur within the fusion zone. Very fine spherical precipitates are observed at the boundaries. For the SHT&A condition, the fracture surface appears different from that in the post-weld aged conditions. The shape of the grains seems rounder, and a uniform distribution of heterogeneous precipitates is present at the boundaries, resulting in interdendritic fracture, Figure 3c. Figure 4 shows the fracture surface of an overaged specimen revealing a uniform distribution of spherical precipitates at the dendrite boundaries that promotes interdendritic fracture.

The fracture mode of the GTA weldments are ductile dimple with secondary cracks at the dendrite boundaries. Failure occurs close to the center of the fusion zone. Figure 5 shows the SEM fractographs of the as-welded, peak aged, and overaged conditions. The as-welded GTA fracture surface is similar to the as-welded EB fracture surface with void formation and slip evident along the dendrite boundaries, Figure 5a. In the peak-aged condition, spherical precipitates decorate the dendrite boundaries, and in the overaged condition, these precipitates become globular, as shown in Figures 5b and 5c. Figure 6 shows the GTA specimen fracture surface after SHT&A for 4 hours. There are three distinct regions: the lamellar microstructures of base metal, the dendrite microstructures of the weld, and the partially melted region (PMR) of the HAZ. Figure 6b shows the PMR identified by smooth surface and various precipitate sizes. PMR is also present on the other fracture surfaces of SHT&A GTA weldments with more pronounced precipitation. Low weldment elongation in SHT&A specimens may have resulted from PMR.

Discussion

Weldability

The results of this study show that in addition to mechanical and chemical cleaning, welding should be done in an inert atmosphere. Visual observation of the EB and GTA fusion zones indicates that they are free of large scale porosity. However, fine porosity appears on some of the EB fracture surfaces viewed with SEM.

Hot cracking of GTA weldments was encountered during the welding procedure development. Hot cracking occurs when the welding mode changes from continuous current to pulsed

current, and when the heat input, i.e. current, is excessive. With proper welding parameters, hot cracking did not occur during GTA welding. Hot cracking did not occur during EB welding. These observations agree with other studies which reported that hot cracking can be reduced by grain refinement in the fusion zone, from columnar grains to equiaxed grains [14]. The advantages of equiaxed grains are that they accommodate contraction strains more easily, and backfill and healing of incipient cracks are more effective[15]. In addition, since hot cracking is an intergranular cracking phenomenon, by having fine equiaxed grains, more energy is required to propagate the crack.

Effect of Grain Size

The grain size dependence on the strength can be predicted using the Hall-Petch relationship [16]. The influence of grain size on strength is small for the range of grain sizes considered. The average dendrite size in the EB fusion zone is 10 μm, and the average dendrite and grain sizes in the GTA fusion zone are 20 μm and 150 μm, respectively, while the average grain size of the base metal is an order of magnitude larger. Assuming that the SHT produced a homogeneous distribution of solutes in the weldments and prior thermal mechanical processing (TMP) of the base metal is erased, the effect of grain size on strength is compared for the SHT&A conditions, see Table 2. For the variation in the grain sizes considered, the strengths of weldments and base metal are quite similar. Thus, the grain size has a limited influence on the strength of the alloy.

Effect of Solute and Precipitate Strengthening

The differences in base metal properties and weldment properties can be explained by their solute/precipitate distribution. TMP is utilized to attain uniform distribution of the solutes in the base metal and to control the formation and distribution of the precipitate phases in the base metal during aging [17]. By influencing the precipitation behavior, a combination of high strength and toughness is obtained. The major strengthening precipitate phases in 2090 are $\delta'(Al_3Li)$, $T_1(AL_2CuLi)$, $\theta'(Al_2Cu)$, and $\beta'(Al_3Zr)$. Among the precipitates that adversely affect the properties are $\delta(AlLi)$ and the iron containing phase, Al_7Cu_4Fe [18,19,20].

For the weldments, prior TMP is erased in the fusion zone. Instead, the degree of solute segregation is established during welding. Since EB welding is a faster cooling rate process than GTA welding, the solute segregation is more limited. Disregarding the effect of microstructure, the effects of solute segregation and consequently precipitate distribution on yield strength are compared between EB and GTA weldments; the difference in yield strength are 70 MPa and 100 MPa in the as-welded and near peak aged conditions, respectively.

In order to quantify solute segregation in the fusion zone of both as-welded EB and GTA weldments, an energy dispersive x-ray line scan was performed across the dendrites. Figure 7 shows the concentration profiles of Al and Cu in the EB fusion zone. Different sensitivity scales were used for Al and Cu due to the large difference in concentrations, 1000 cps and 100 cps, respectively. The Al concentration profile shows Al depleted regions across the dendrite boundaries and at precipitates. The Cu concentration profile of the same line contains Cu peaks across the boundaries but not at the precipitates. For the GTA fusion zone analysis, Zr was also analyzed since Al depleted regions are present without the corresponding Cu peaks. The same sensitivity

scales were used as in the previous analysis. Figure 8a shows the concentration profiles of Al and Cu. The Al valleys and Cu peaks are better defined in the GTA fusion zone but the profiles are similar to those in the EB fusion zone. Figure 8b shows the concentration profiles of Al and Zr within the same region. The Al concentration profile is the same as in Figure 8a. The Zr concentration profile exhibits no definite peaks until the line intersects one of the precipitates and then the concentration reaches a maximum, indicating the presence of Zr-containing precipitates at the boundary. On aging these Cu and Zr concentration gradients at the boundaries form precipitate gradients across the boundaries and establish precipitate-free regions within the dendrites.

In order to further characterize the effect of aging on precipitation behavior within the fusion zone, TEM was done on the as-welded, peak-aged and SHT&A GTA welds. There is some controversy regarding the exact composition of the plate-like precipitate phases [18,20]. For the purpose of this paper, the distribution of these plate-like precipitates is more important, and they will be merely described as plate-like precipitates. Figure 9 shows the bright field image of the as-welded specimen in the [110] orientation. The SAD pattern shows superlattice diffraction spots that confirm the presence of δ' and β' phases. In addition, atomic absorption spectroscopy was utilized to analyze for lithium in the bulk, and the analysis indicated no lithium loss from the weld. The micrograph reveals the distribution of dislocations, and δ' and β' phases, but no plate-like precipitates are found. Tosten, et al. [18] have found similar results in their as-quenched base metal specimen, where inhomogeneous dispersion of Al_3Zr and very fine distribution of δ' were present, but no evidence of θ', T_1, δ was found. Figure 10 shows the bright field image of peak-aged specimen in the [100] orientation. The micrograph shows a fine distribution of δ' phase and a non-uniform distribution of plate-like precipitate phases around the boundary. Large spherical precipitates are also found at the boundaries. Figure 10 shows the bright field image of the SHT&A specimen in the [211] orientation. The micrograph reveals a uniform distribution of plate-like precipitates as well as δ' and a random distribution of β'. In addition, plate-like precipitates are present at the dendrite boundaries.

The results of the TEM analysis indicate that the distribution of precipitates is associated with the deterioration in weldment strength and elongation. In the as-welded condition, no plate-like precipitates are found in the fusion zone, which limits the strength of the weldments. On the other hand, the as-welded condition shows a limited dendrite boundary precipitation, which may explain the higher elongation of the as-welded specimens. In the peak-aged condition, the non-uniform distribution of precipitates in the fusion zone appears to be the cause for the lower weldment strength than that of the base metal. The higher strength of the SHT&A weldments is associated with a homogeneous distribution of the plate-like precipitates in the fusion zone. However, as the aging time increases, heterogeneous precipitation also occurs at the dendrite boundaries. There is a variation in the precipitate morphology with the heat treatment. In the postweld aged condition, the precipitate morphology is globular as a result of solute segregation, and in the SHT&A condition the precipitate morphology changes to plate-like, influencing the weldment elongation differently. The presence of the plate-like precipitates at the dendrite boundaries has a less adverse effect on the weldment elongation than that of the globular precipitates. The plate-like precipitates seem to be coherent in habit plane while the globular precipitates are probably incoherent.

Conclusions

The weldability of 2090 is studied along with the metallurgical changes associated with welding and aging. The following conclusions are drawn.

1) Porosity can be controlled by machining and chemically cleaning the surfaces and welding in an inert atmosphere. Hot cracking can be eliminated by use of proper welding parameters.

2) The best aging temperature for the base metal and EB weldments is 160°C resulting in a 75% joint efficiency and for the GTA weldment is 190°C resulting in a 55% joint efficiency. Aging at 230°C leads to a serious deterioration in the properties.

3) The strength of the EB weldments is higher than that of the GTA weldments, perhaps because of the difference in the solute distribution and consequently, the precipitate distribution. Grain size has a limited influence on the strength of the alloy.

4) Weldment elongation is significantly lower than that of the base metal. The deterioration is associated with precipitation at the dendrite boundaries.

Acknowledgement

The authors would like to thank Aluminum Company of America for providing the material and B. Olsen of Lawrence Livermore National Laboratory for producing the EB welds. This work is supported by the Director, Office of Energy Research, Office of Fusion Energy, Development and Technology Division of the U.S. Department of Energy under contract #DE-AC03-76SF00098.

References

1. Glazer, J., Verzasconi, S.L., Dalder, E.N.C., Yu, W., Emigh, R.A., Ritchie, R.O., Morris, J.W., Adv. Cryo. Eng., 32, pp. 397-404 (1986).

2. Glazer, J., Verzasconi, S.L., Sawtell, R.R., and Morris, J.W., Metall. Trans., 18A, pp. 1695-1701 (1986).

3. Bokshtein, C.A., et al, Avtom. Svarka, 6, 34 (1978).

4. Ishchenko, A. Ya, and Chayun, A.G., Second International Conference on Aluminum Weldments, Munich, F.R.G. (1982), paper I.10.

5. Staley, J.T., Rioja, R.J., Wyss, R.K., and Liu, J., Alcoa Laboratory Technical Center Division Report 04-87-KD-34-56 (1987).

6. Shamrai, F.M., Izd., Zn USSR, (1954).

7. Pickens, J.R., Journal of Materials Science, 20 , pp. 4247-4258 (1985).

8. Pickens, J.R., Langan, T.J., and Barta, E., Aluminium-Lithium Alloys III, Proceedings of Aluminum-Lithium Conference, eds. C. Baker, P.J. Gregson, S.J. Harris, and C.J. Peel, The Institute of Metals, pp. 137-147 (1985).

9. Pumphrey, W.I., Jennings, P.H., Journal Institute of Metals, 75, pp. 235-256 (1948).

10. Cross, C.E., Olsen, D.L., Edwards, G.R., and Capes, J.F., Aluminium-Lithium Alloys II, Proceedings of Aluminum-Lithium Conference, eds. T.H. Sanders, Jr. and E.A. Starke, Jr., The Metallurgical Society of AIME, pp. 675-682 (1983).

11. Pumphrey W.I., and Lyons, J.V., Journals Institute of Metals, 74, pp. 439-455 (1948).

12. Borland, J.C., British Welding Journal, 8, pp. 508-512 (1960)

13. Clyne, T.W., and Davies, G.J., TMS Proc. Int. Conf. Solidification, pp. 275-278 (1977).

14. Lees, K.C.G., Journal Institute of Metals, 72, 343 (1946).

15. Spencer, D., Mehrabian, R., and Flemings, M.C., Met. Trans., 3,1925 (1972).

16. Dollar, M., and Thompson, A.W., Acta Metall., 35, 1, pp. 227-235 (1987).

17. Rioja, R.J., Bretz, P.E., Sawtell, R.R., Hunt, W.H., and Ludwiczak, E.A., Aluminum Alloys Their Physical and Mechanical Properties, Vol. III, Conf. Proc., eds. E.A. Starke, Jr. and T.H. Sanders, Jr., Engineering Materials Advisory Service LTD., pp. 1781-1797 (1986).

18. Tosten, M.H., Vasudevan. A.K., and Howell, P.R., Aluminium-Lithium Alloys III, Proceedings of Aluminum-Lithuim Conference, eds. C. Baker, P.J. Gregson, S.J. Harris, and C.J. Peel, The Institute of Metals, pp. 490-495 (1985).

19. Tosten, M.H., Vasudevan. A.K., and Howell, P.R., Aluminium-Lithium Alloys III, Proceedings of Aluminum-Lithium Conference, eds. C. Baker, P.J. Gregson, S.J. Harris, and C.J. Peel, The Institute of Metals, pp. 483-489 (1985).

20. Rioja, R.J., and Ludwiczak, E.A., Aluminium-Lithium Alloys III, Proceedings of Aluminum-Lithium Conference, eds. C. Baker, P.J. Gregson, S.J. Harris, and C.J. Peel, The Institute of Metals, pp. 471-482 (1985).

List of Tables

Table 1: Welding parameters.

Table 2: Tensile test results.

Heat Treatment (°C/Hours)	EBW /GTAW/BM 0.2% Yield Strength (MPa)	EBW/GTAW/BM UTS/FS*[5] (MPa)	EBW/GTAW/BM % Total Elongation (25.4 mm gage length)
PWA[1]			
160/8	341 / 230 / 501	380* / 292 / 572	0.6 / 1.2 / 8.9
160/16	- / 262 / 538	- / 314* / 583	- / 0.8 / 9.4
160/32	413 / 282 / 549	436* / 342* / 574	0.2 / 0.8 / 9.4
190/2	307 / - / -	313* / - / -	0.3 / - / -
190/4	337 / 266 / 474	360* / 325* / 520	0.5 / 0.7 / 8.8
190/16	345 / 307 / 476	361* / 345* / 527	0.3 / 0.5 / 11.2
190/24	- / 307 / -	- / 345* / -	- / 0.5 / -
230/2	- / 219 / -	- / 276 / -	- / 1.2 / -
230/4	294 / 232 / 316	333* / 293* / 394	0.7 / 1.0 / 11.0
230/16	254 / 224 / 247	302* / 276* / 339	1.3 / 1.2 / 7.8
SHT & A[2]			
160/4	284 / 284 / 287	387* / 365* / 334*	5.4 / 2.5 / 6.9
160/16	388 / 355 / 381	450* / 401* / 453*	1.8 / 1.1 / 10.1
Base Metal Temper[3]			
T3	176 / 103 / 279	268 / 245 / 345	4.4 / 4.4 / 11.2
T8	186 / 131 / 549	258* / 247* / 564	1.3 / 3.6 / 9.4
All Weld Metal[4]			
As-Welded	- / 125 / -	- / 237 / -	- / 17.0 / -
160/32	- / 236 / -	- / 303 / -	- / 1.5 / -

[1] PWA: post weld aged.
[2] SHT &A: post weld solution heat treated and aged.
[3] As-welded.
[4] See Figure 1b.
[5] FS*: fracture strength.

	GTAW	EBW
Current:	110 A	9.5 mA
Voltage:	18-20 V	80 kV
Travel speed:	6.4 mm/s	16.9 mm/s
Electrode diameter:	2.4 mm	-
Electrode angle:	90-120 deg	-
Electrode to work distance:	1.6 mm	280 mm
Shielding gas:	75% He-25% Ar	
Vacuum pressure:		2×10^{-4} Torr

List of Figures

Figure 1: Tensile specimen configuration: a) composite specimen; b) all-weld metal specimen. Dimensions are in mm, and the shaded regions represent the fusion zone.

Figure 2: SEM fractographs of base metal: a) aged at 160°C for 16 hours; b) aged at 230°C for 16 hours.

Figure 3: SEM fractographs of EB weldments: a) as-welded condition; b) aged at 160°C for 32 hours; c) solution heat treated and aged at 160°C for 16 hours.

Figure 4: SEM fractograph of EB weldment aged at 230°C for 16 hours.

Figure 5: SEM fractographs of GTA weldments: a) as-welded condition; b) aged at 190°C for 160 hours; c) aged at 230°C for 16 hours.

Figure 6: SEM fractographs of GTA weldment in solution heat treated and aged at 160°C for 4 hours: a) overall fracture surface; b) partially melted region.

Figure 7: EDX line scan of Al and Cu in the EB fusion zone.

Figure 8: EDX line scan of the GTA fusion zone: a) concentration profiles of Al and Cu; b) concentration profiles of Al and Zr.

Figure 9: TEM bright field image of as-welded GTA fusion zone; [110] orientation.

Figure 10: TEM bright field image of peak-aged GTA fusion zone; [100] orientation.

Figure 11: TEM bright field image of solution heat treated and aged GTA fusion zone; [211] orientation.

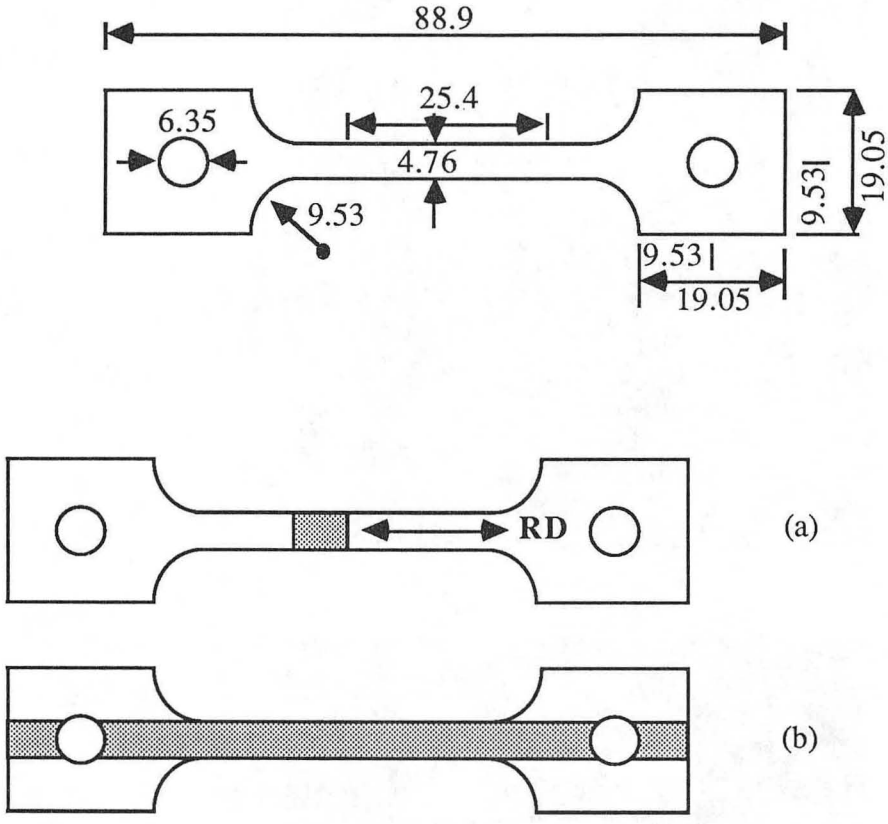

Figure 1

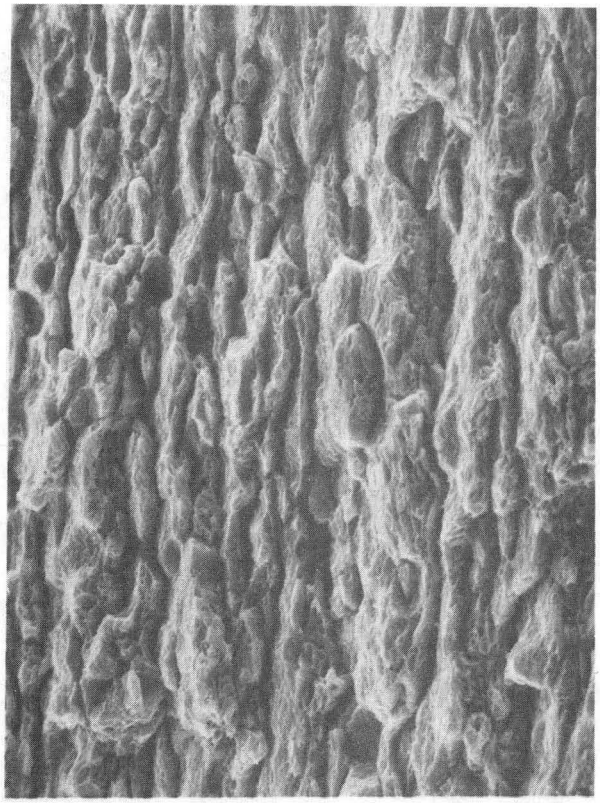

10 µm

(b)

10 µm

(a)

XBB883-2251

Figure 2

(a)

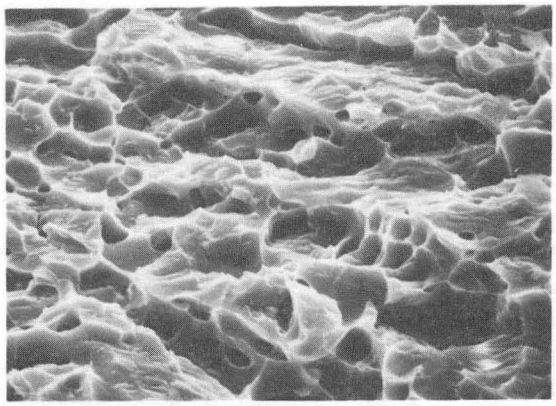

(b)

(c)

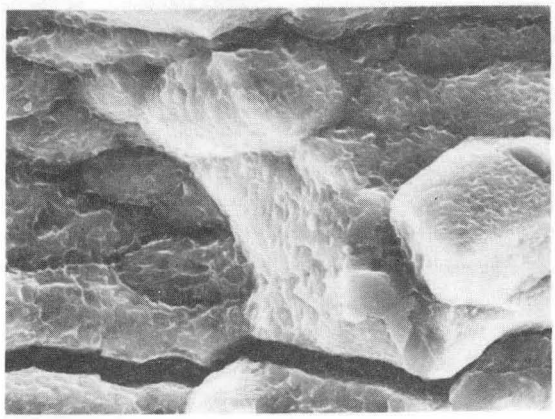

XBB 883--2256

4 μm

Figure 3

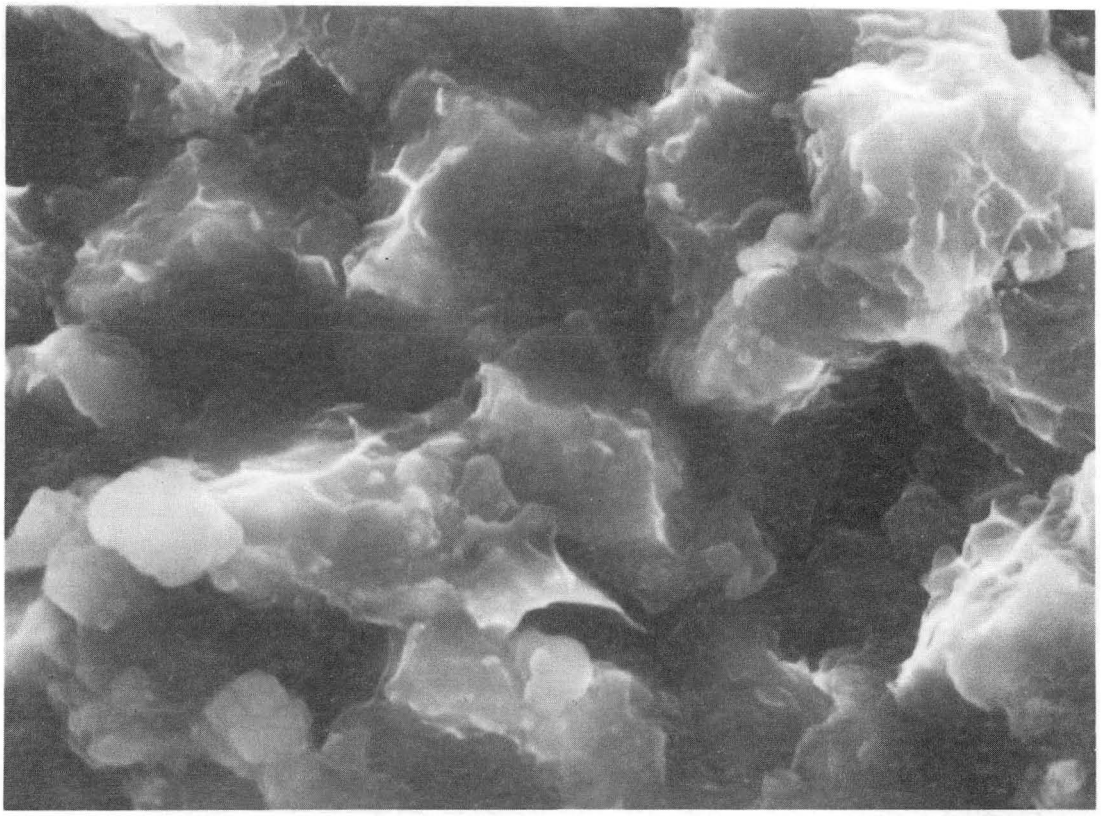

XBB 883-2250

2 μm

Figure 4

(a)

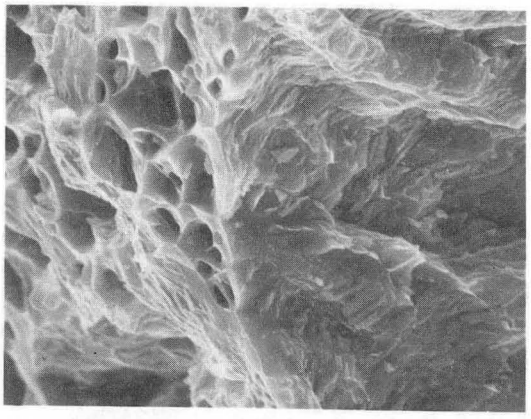

(b)

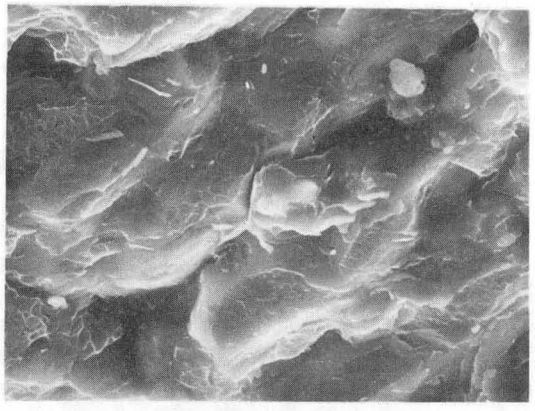

(c)

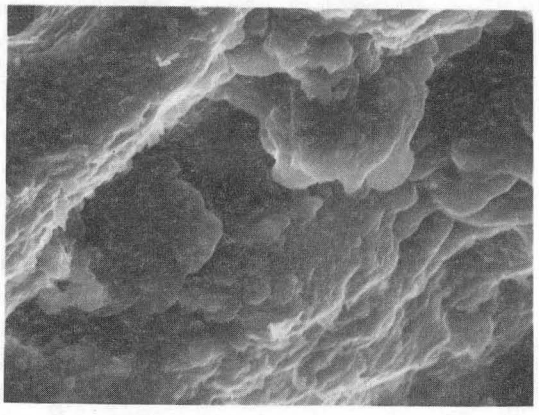

XBB 883-2253

4 μm

Figure 5

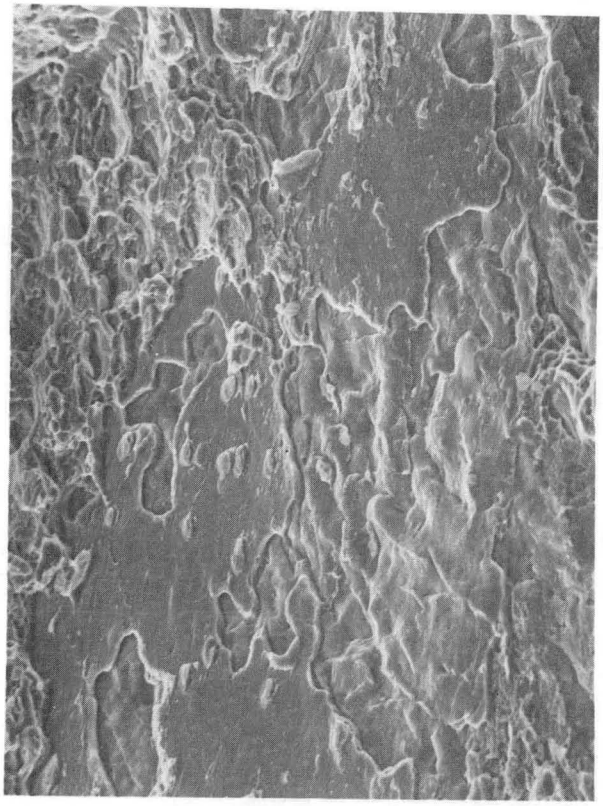

25 µm

(b)

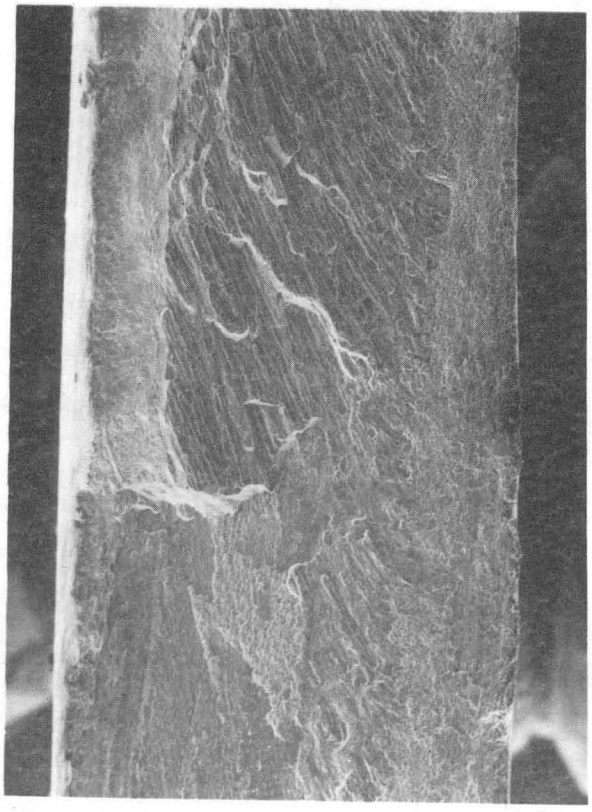

360 µm

(a)

XBB 879-8277A

Figure 6

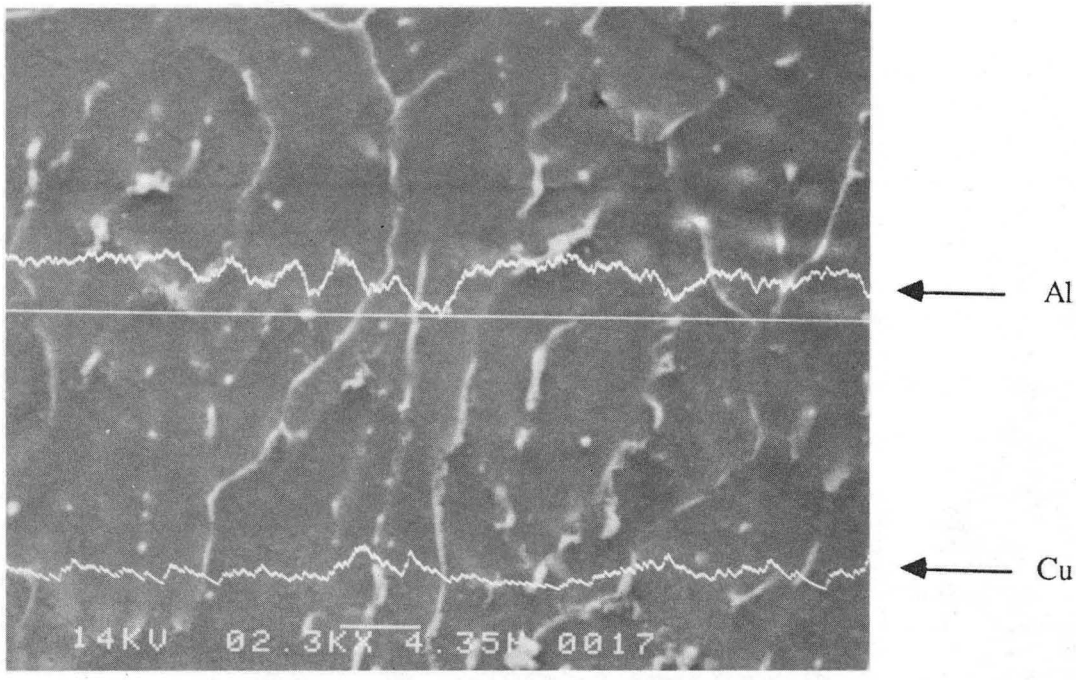

XBB 883-2257

Figure 7

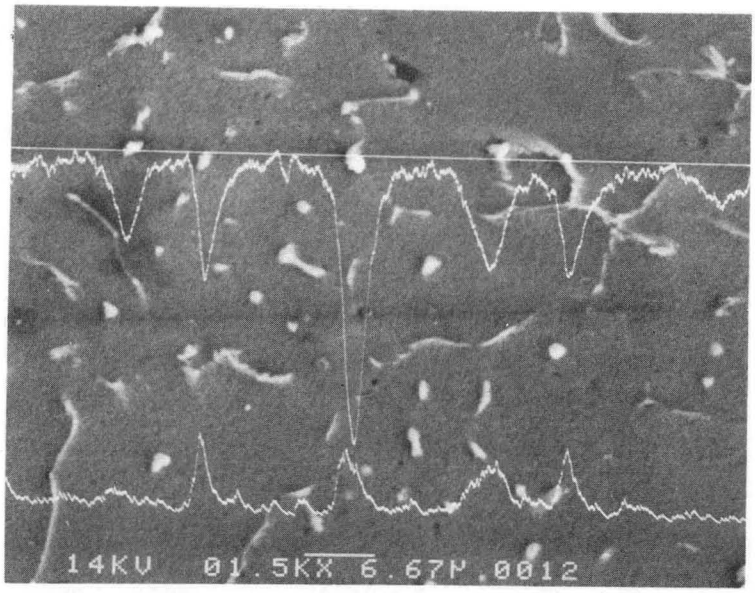

Al

(a)

Cu

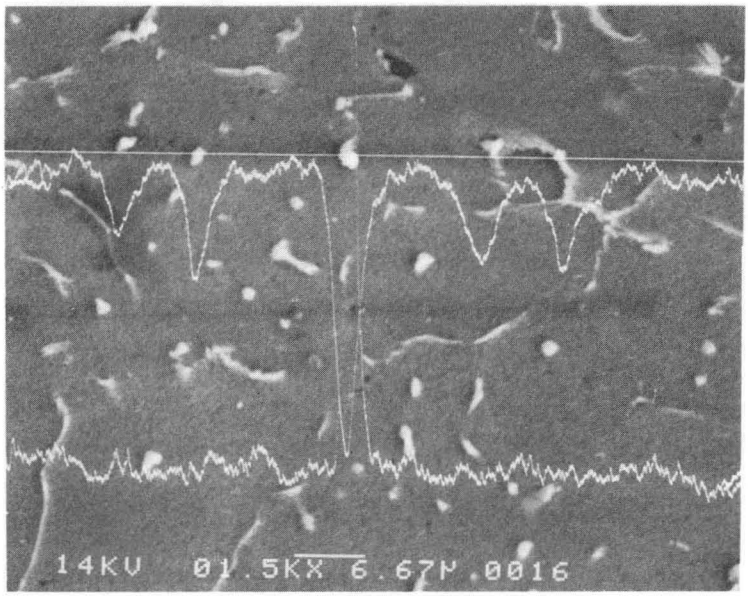

Al

(b)

Zr

XBB 883-2252

Figure 8

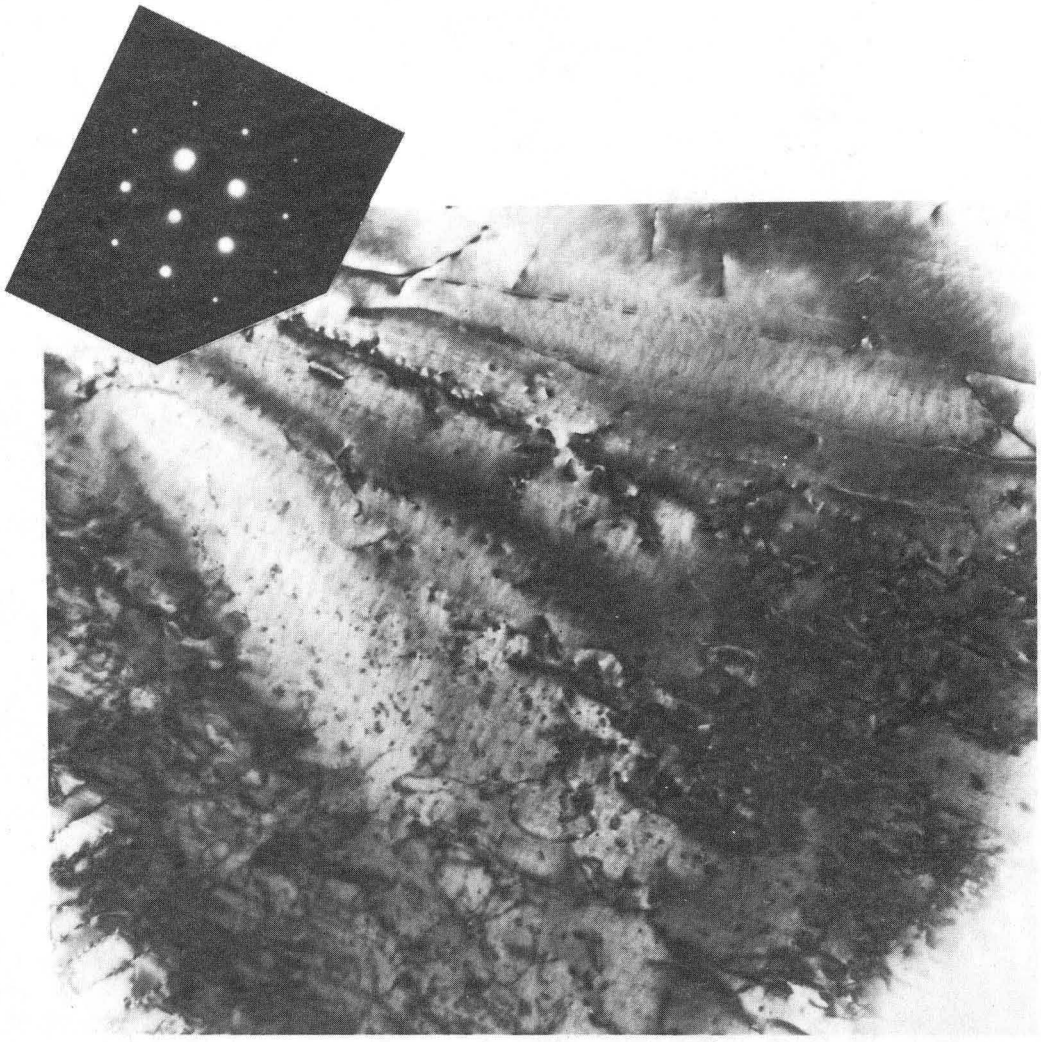

200 nm

XBB 883-2254

Figure 9

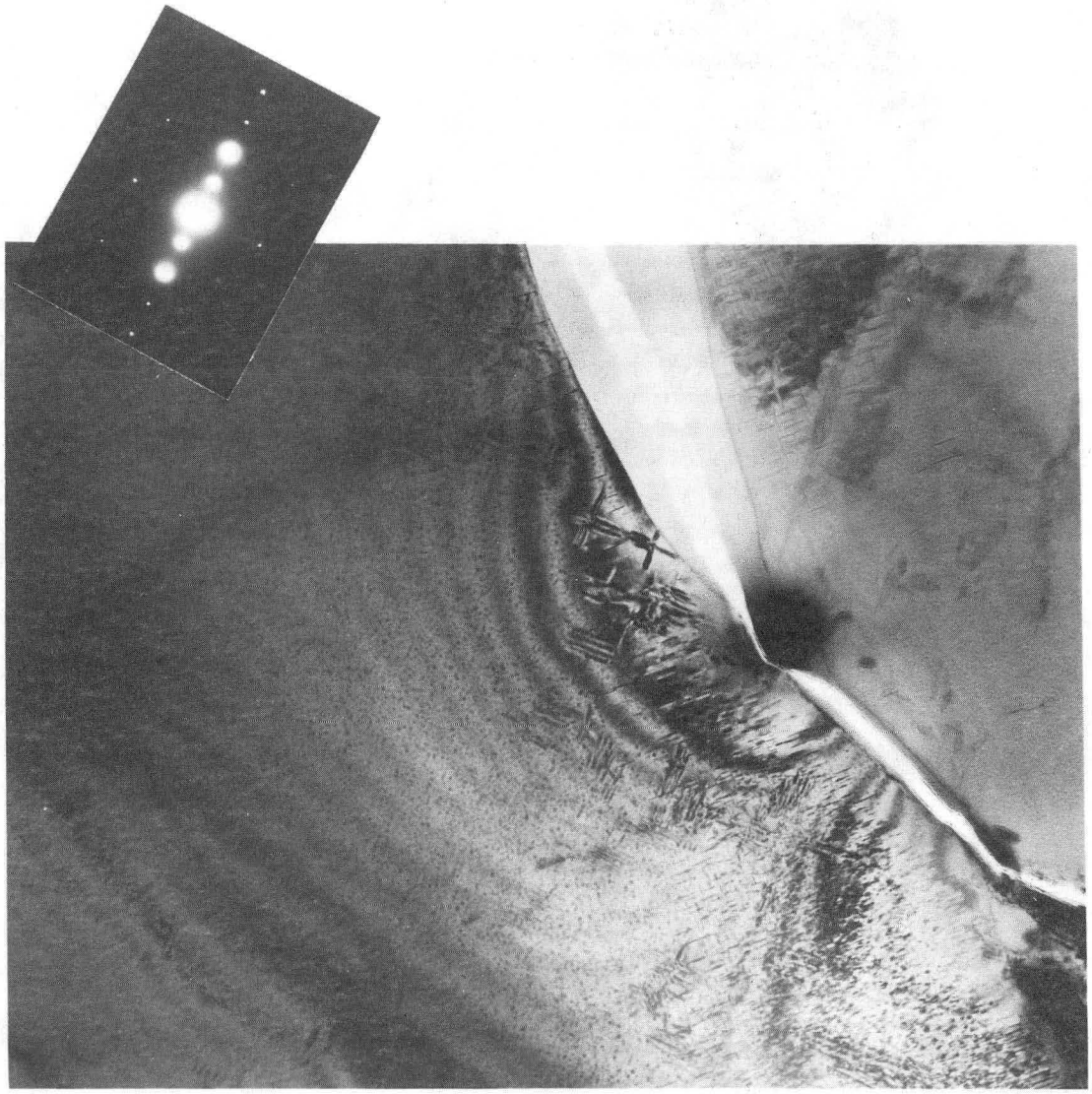

200 nm

XBB 883-2249

Figure 10

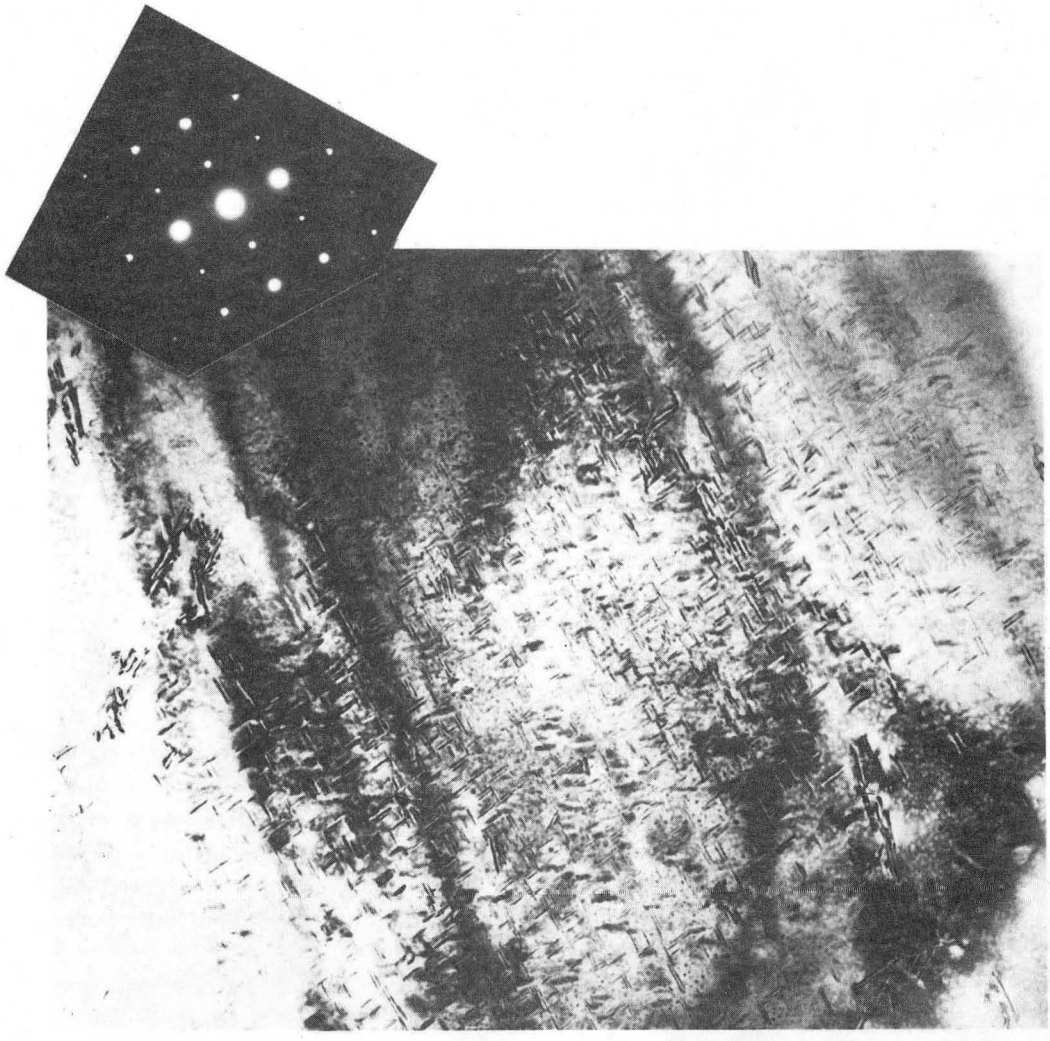

90 nm

XBB 883-2255

Figure 11

LAWRENCE BERKELEY LABORATORY
TECHNICAL INFORMATION DEPARTMENT
UNIVERSITY OF CALIFORNIA
BERKELEY, CALIFORNIA 94720